Electronic Supplementary Information

0D MXene quantum dots/2D MXene derived metal-organic frameworks for enhanced nonlinear optical absorption across spectral and temporal regimes†

Naying Shan,[a] Zhiyuan Wei,[a] Zihao Guan,[a] Yang Zhao,[a] Fang Liu,[a] Lulu Fu,[a] Yanyan Xue,[b] Zhipeng Huang,[a] Mark G. Humphrey,[c] Jun Xu,[b] and Chi Zhang[a,*]

[a] *China-Australia Joint Research Center for Functional Molecular Materials, School of Chemical Science and Engineering, Tongji University, Shanghai 200092, China. E-mail: chizhang@tongji.edu.cn*

[b] *School of Physical Science and Engineering, Tongji University, Shanghai 200092, China*

[c] *Research School of Chemistry, Australian National University, Canberra, Australian Capital Territory 2601, Australia*

1. Experimental Procedures

1.1. Preparation of TPPCOOMe. Methyl 4-formylbenzoate (0.086 mol, 14.41 g) was fully dissolved in propionic acid (250 mL) at 60 ºC in the 500 mL two-necked flask. Pyrrole (0.086 mol, 6.09 mL) in propionic acid (20 mL) was added dropwise. Then the mixture was refluxed for 12 h. After the reaction, the mixture was cooled to room temperature. The precipitates were obtained by suction filtration and washed with ethanol (EtOH), ethyl acetate (EA), and tetrahydrofuran (THF), respectively. The collected precipitates were dried in an oven for 12 h, and a purple powder as meso-tetra(4-carboxy-phenyl) porphyrin 5,10,15,20-tetrakis(4-methoxycarbonylphenyl) porphyrin (TPPCOOMe) was obtained (4.9 mmol, 4.2 g, yield 23%).1H NMR (400 MHz, $CDCl_3$-*d*, TMS, δ/ppm): 8.80 (s, 8H), 8.43 (dt, 8H, *J* = 8 Hz), 8.28 (dt, 8H, *J* = 8 Hz), 4.14 (s, 2H), 4.09 (s, 10H), –2.83 (s, 2H).

1.2. Preparation of TCPP. The obtained TPPCOOMe (0.75 g) was stirred in a mixture of THF (25 mL) and methanol (MeOH) (25 mL), to which a solution of sodium hydroxide (2.40 g, 60.00 mmol) in H_2O (25 mL) was introduced. Then the mixture was refluxed for 12 h. After the reaction, the mixture was cooled to room temperature. THF and MeOH were evaporated. Additional water was added to the resulting aqueous phase and the mixture was heated until the solid was fully dissolved. Then the solution was acidified with 1 M hydrochloric acid (HCl) until no further precipitate was detected. The precipitate was washed with water, collected by centrifugation, and dried under vacuum for obtaining the product of meso-tetra(4-carboxy-phenyl) porphyrin (TCPP) (0.84 mmol, 0.66 g, yield 96%). 1H NMR (400 MHz, DMSO-d_6, TMS, δ/ppm): 8.86 (s, 8H), 8.38 (d, 8H), 8.34 (d, 8H), –2.94 (s, 2H).

1.3. Preparation of V_2C MXene. 1 g of V_2AlC MAX powder (200 mesh) was immersed in 20 ml of hydrofluoric acid (HF) (40%) and stirred at 35 ºC for 96 hours. Wash the mixture with deionized water and centrifuged (3000 r.p.m) to collect the sediment. The washing procedure was repeated until the pH of the supernatant reaches approximately 6. The V_2C was obtained by filtration.

1.4. Preparation of d-V_2C MXene. As-etched sediment V_2C MXene was immersed in 10 mL of tetramethylammonium hydroxide (TMAOH) and stirred for 24 hours at room temperature for delamination. Subsequently, separate the supernatant by centrifugation to obtain clay-like sediment, namely, d-V_2C MXene.

1.5. Preparation of Ti_3C_2 MXene. The Ti_3AlC_2 powder was etched to remove the Al layers by HF to obtain Ti_3C_2 nanosheets. First, 1 g of Ti_3AlC_2 MAX (200 mesh) powder was added to 20 mL of HF (40%) and stirred for 48 hours at room temperature. Wash the obtained powder with ethanol and deionized water several times by centrifugation at 9000 rpm. The washing

procedure was repeated until the pH of the supernatant reaches approximately 6. After discarding the supernatant, the Ti_3C_2 nanosheets were freeze-dried in a vacuum overnight.

1.6. Preparation of Ti_3C_2 QD. The Ti_3C_2 MXene nanosheets were placed in 80 mL of N, N-dimethylformamide (DMF) and ultrasonicated for half an hour. Transfer the mixture to a 100 mL Teflon autoclave at 150 °C for 6 hours. Finally, Ti_3C_2 QD was obtained by filtration through a 0.22 μm membrane.

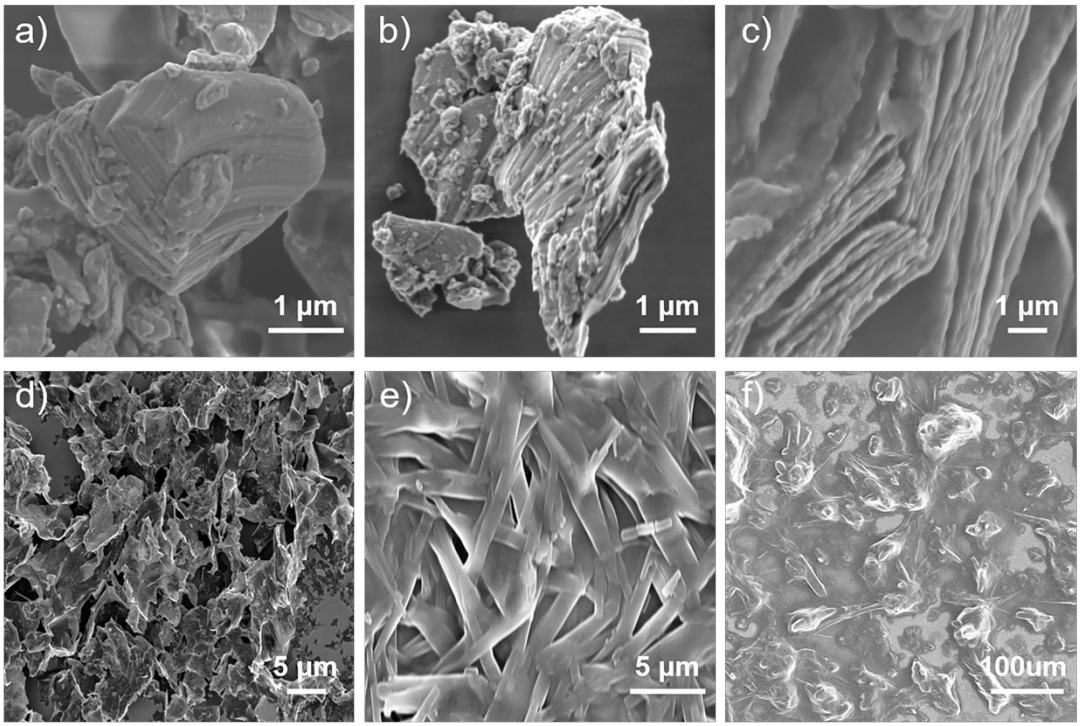

Figure S1. Scanning electron microscope (SEM) images of (a) V_2AlC, (b) Ti_3AlC_2, (c) d-V_2C MXene, (d) Ti_3C_2 MXene, (e) V_2C PMOF, and (f) Ti_3C_2 QD/V_2C PMOF.

d-V_2C		Ti_3C_2 QD		V_2C MOF		Ti_3C_2 QD/V_2C MOF	
Element	Atom (%)	Element	Atom (%)	Element	Atom (%)	Element	Atom (%)
C 1s	56.25	C 1s	48.74	C 1s	77.23	C 1s	59.85
O 1s	29.39	O 1s	22.48	O 1s	16.64	O 1s	20.43
V 2p	10.39	Ti 2p	17.46	V 2p	2.00	V 2p	0.41
F 1s	3.98	F 1s	11.32	N 1s	4.13	F 1s	6.01
						Ti 2p	12.00
						N 1s	1.29

Table S1. The atomic percentages in corresponding samples.

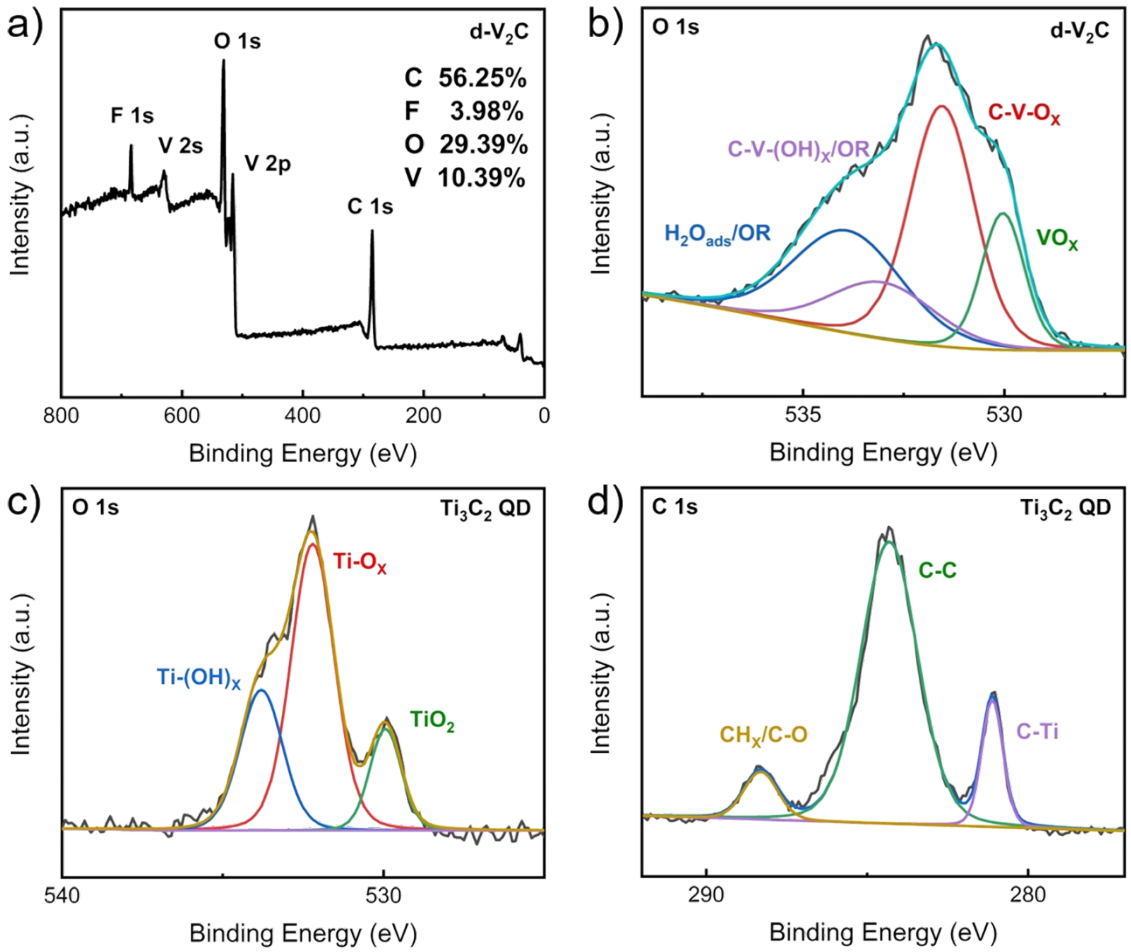

Figure S2. (a) Survey X-ray photoelectron spectroscopy (XPS) spectrum of d-V_2C. High-resolution XPS spectra of (b) O 1s in d-V_2C MXene. The O 1s region revealed the presence of VO_x (~ 530.0 eV), C–V–O_x (~ 531.5 eV), C–V–$(OH)_x$ (~ 533.1 eV), and H_2O_{ads} (~ 534.1 eV). High-resolution XPS spectra of (c) O 1s and (d) C 1s in Ti_3C_2 QD. The O 1s region consisted of three components, corresponding to TiO_2 (~ 529.9 eV), C–Ti–O_x (~ 532.2 eV), and Ti–$(OH)_x$ (~ 533.8 eV), which confirmed the surface terminations of O species. Correspondingly, the C 1s region was fitted by three peaks, about C–Ti (~ 281.1 eV), C–C (~ 284.3 eV), and CH_x/C–O (~ 288.3 eV).

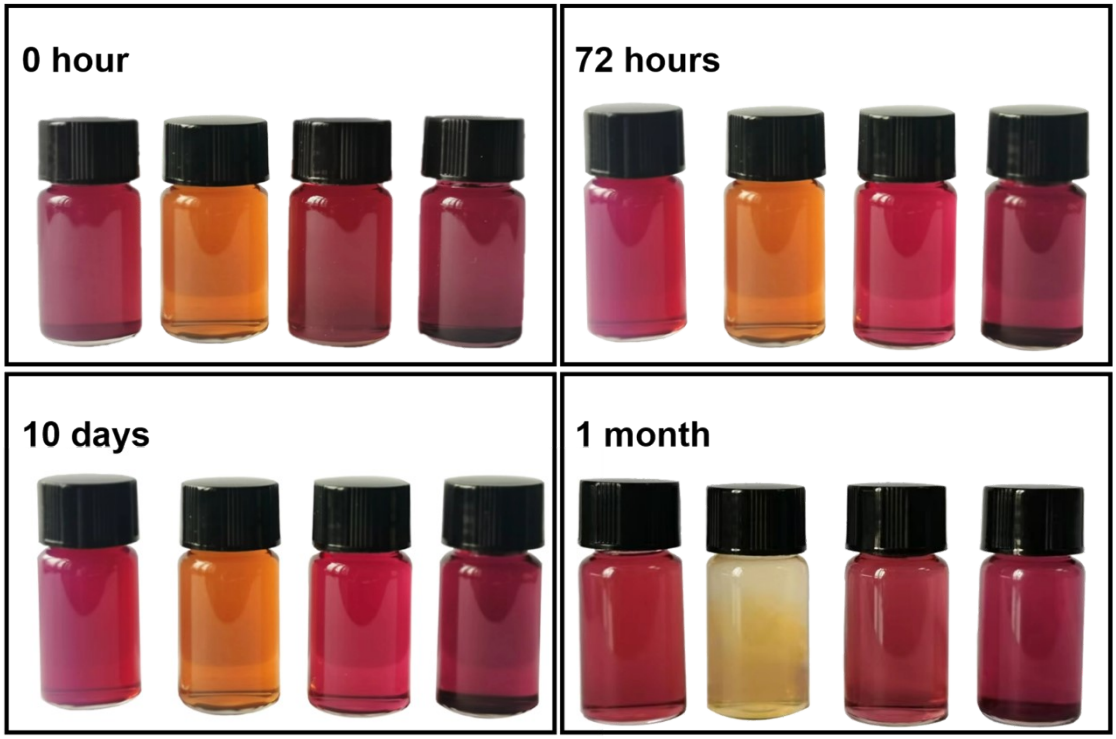

Figure S3. Photographs of TCPP, Ti_3C_2 QD, V_2C PMOF, and Ti_3C_2 QD/V_2C PMOF dispersions with all concentrations at 0.1 mg/mL. The first photograph exhibits the fresh dispersions after sonication for 10 minutes; the following parts show the dispersions after storage for 72 hours, 10 days, and 1 month.

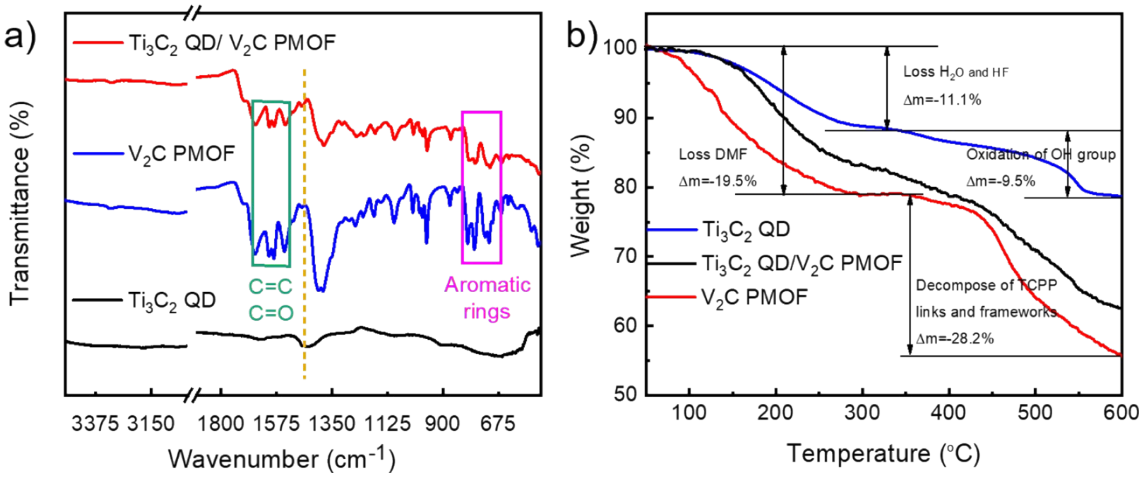

Figure S4. (a) Fourier transform infrared spectra (FTIR) of Ti_3C_2 QD, V_2C PMOF, and Ti_3C_2 QD/V_2C PMOF. The N–H stretching vibration and in-plane vibration peaks are observed at 3311 and 964 cm^{-1} in V_2C PMOF, as well as at 3316 and 963 cm^{-1} in Ti_3C_2 QD/V_2C PMOF hybrids. Moreover, C–H bending vibrations of the organic ligands TCPP are confirmed in V_2C PMOF (1382 cm^{-1}) and Ti_3C_2 QD/V_2C PMOF (1398 cm^{-1}), respectively. (b) Thermal gravimetric analysis (TGA) of Ti_3C_2 QD, V_2C PMOF, and Ti_3C_2 QD/V_2C PMOF. The first phase corresponds to the separation and loss of the solution DMF, while the second phase corresponds to the decomposition of the organic components TCPP and frameworks, occurring from 350 °C with an abrupt weight loss. The decomposition of Ti_3C_2 QD mainly occurs in two phases: the first stage corresponds to the loss of molecules (water and HF) and the second phase originates from oxidized OH groups. All of these processes occur in the heterostructure Ti_3C_2 QD/V_2C PMOF.

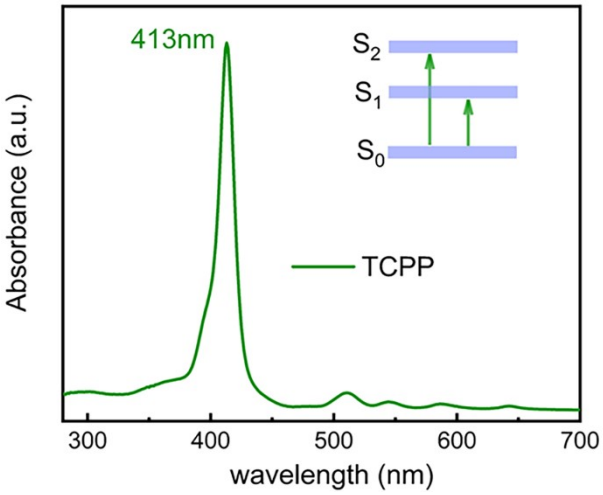

Figure S5. Ultraviolet-visible (UV-Vis) absorption spectrum of TCPP.

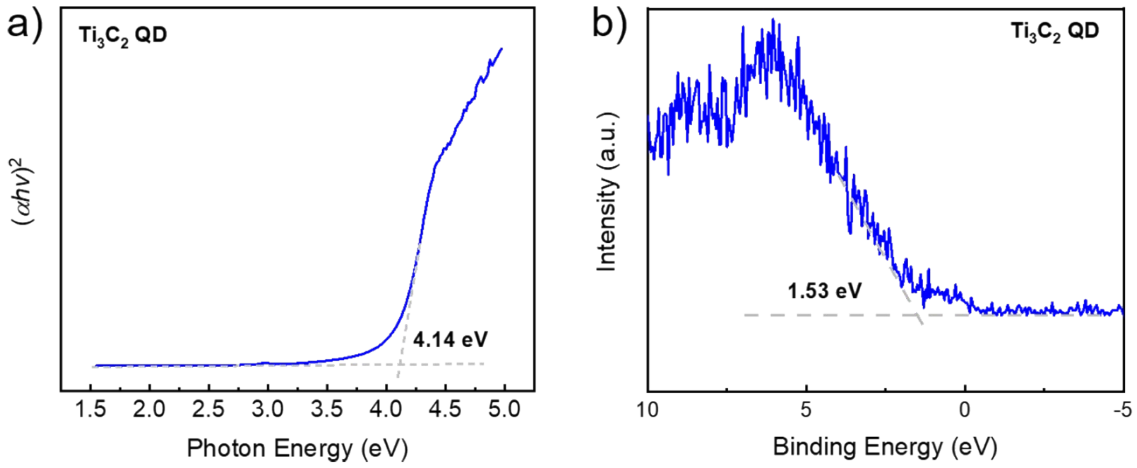

Figure S6. (a) The bandgap calculated by Tauc plot of Ti_3C_2 QD. (b) To determine the valence band (VB), XPS-VB spectra of Ti_3C_2 QD are plotted.

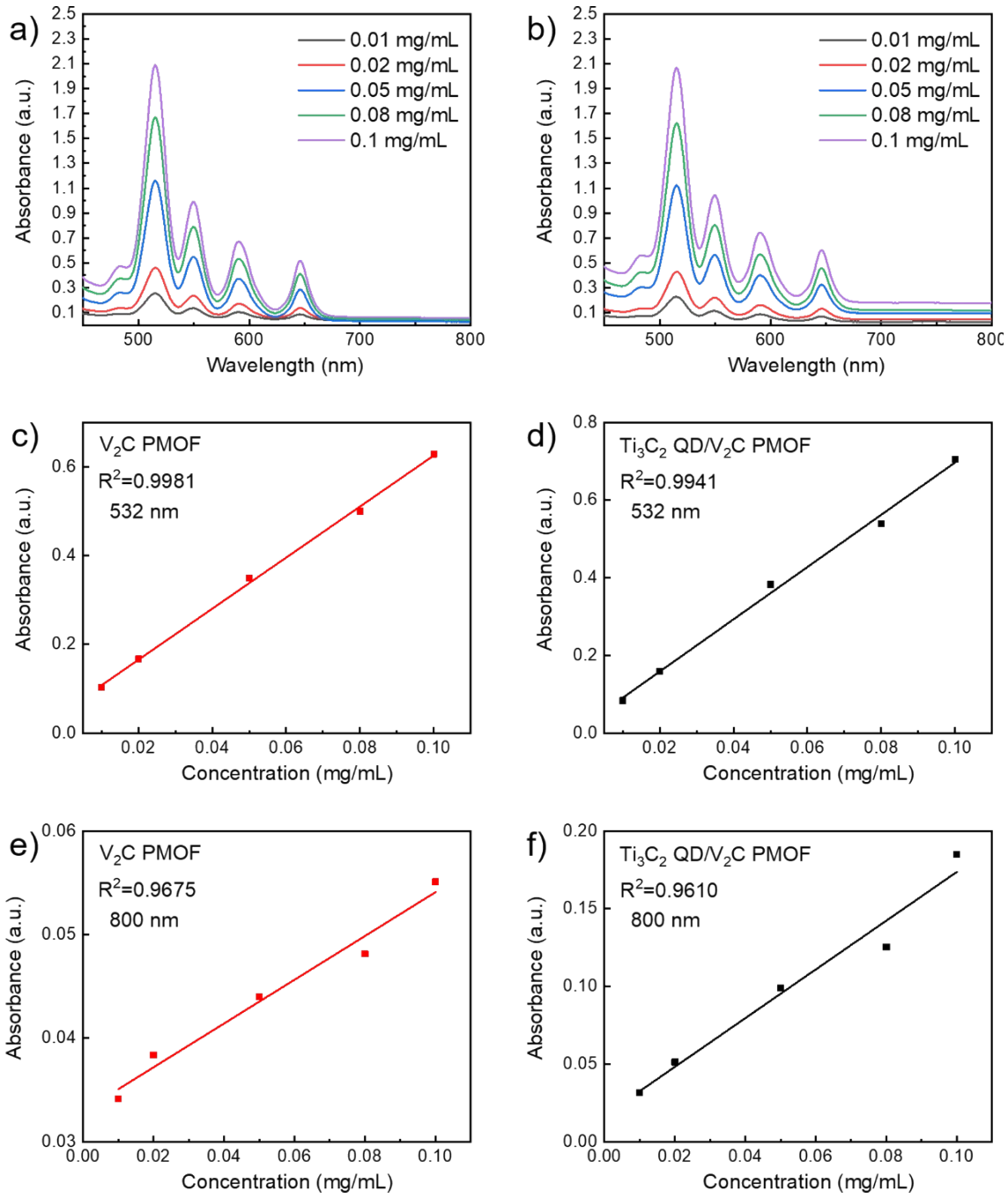

Figure S7. The absorption spectra of (a) V_2C PMOF and (b) Ti_3C_2 QD/V_2C PMOF at different concentrations. The absorbance of (c) V_2C PMOF and (d) Ti_3C_2 QD/V_2C PMOF at different concentrations under the irradiation of 532 nm. The absorbance of (e) V_2C PMOF and (f) Ti_3C_2 QD/V_2C PMOF at different concentrations under the irradiation of 800 nm. The straight lines are the linear fitting results of the data.

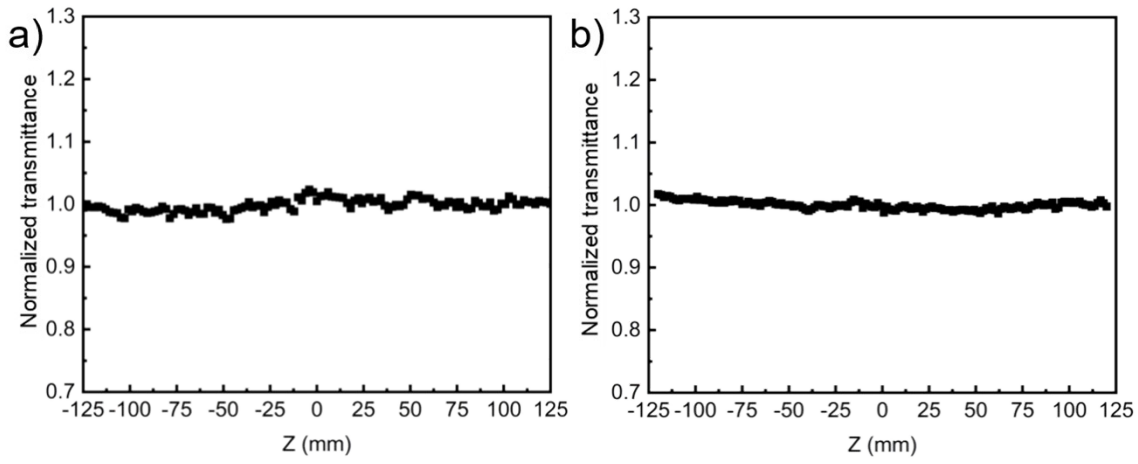

Figure S8. Open aperture Z-scan curves for blank solvent DMF (a) in the nanosecond (ns) regime of 532 nm under input fluence energy of 110 μJ and (b) in the femtosecond (fs) regime of 800 nm under input fluence energy of 60 nJ.

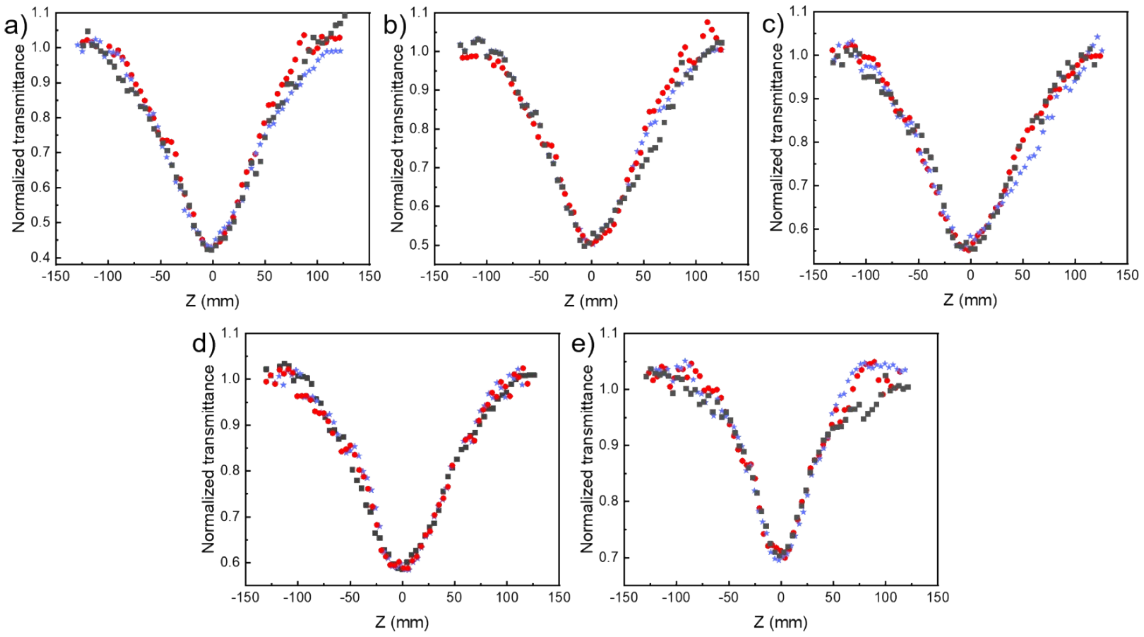

Figure S9. Open aperture Z-scan results of V_2C PMOF in the ns regime of 532 nm at different incident pulse energies of (a) 110 μJ, (b) 90 μJ, (c) 70 μJ, (d) 50 μJ, and (e) 30 μJ pulsed light for the 0 hour, 72-hour, and 10-day storage.

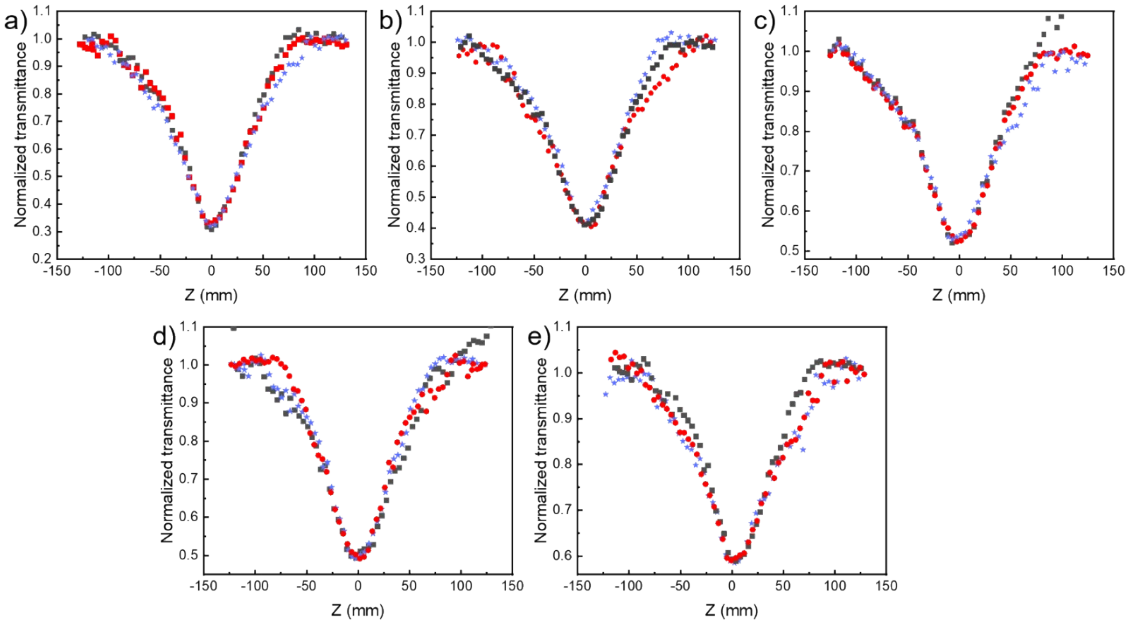

Figure S10. Open aperture Z-scan results of Ti_3C_2 QD/V_2C PMOF in the ns regime of 532 nm at different incident pulse energies of (a) 110 μJ, (b) 90 μJ, (c) 70 μJ, (d) 50 μJ, and (e) 30 μJ pulsed light for the 0 hour, 72-hour, and 10-day storage.

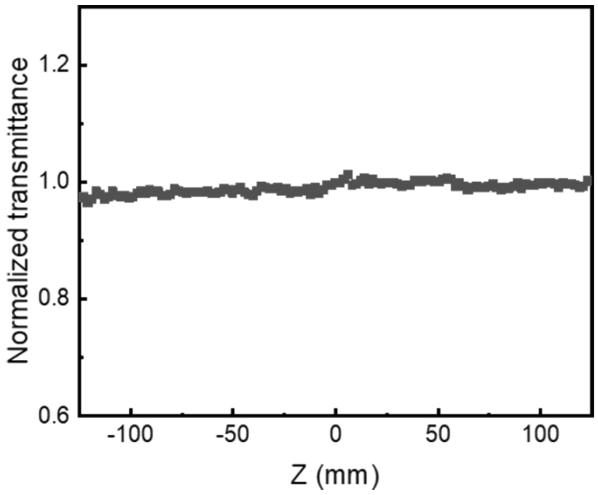

Figure S11. Open aperture Z-scan results of Ti_3C_2 QD/V_2C PMOF in the ns regime of 1064 nm.

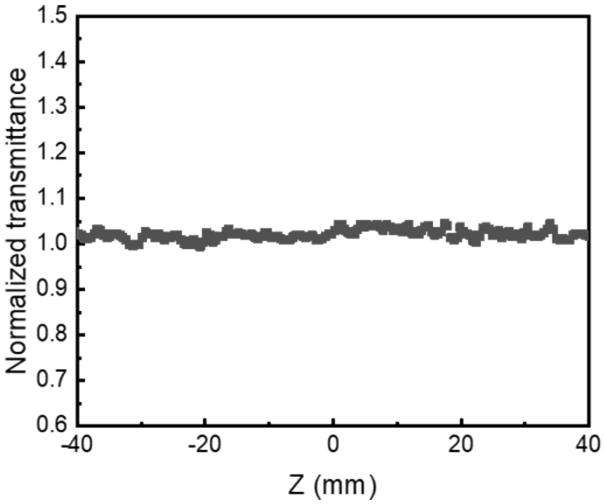

Figure S12. Open aperture Z-scan results of Ti_3C_2 QD/V_2C PMOF heterostructure in the fs regime of 1030 nm.

Table S2. Performance comparison of optical limiting threshold.

Samples	λ (nm)	F_{OL} (J cm^{-2})
TPP[1]	532	33
PIZA-1[2]	532	5.04
C_{60}@PIZA-1[2]	532	5.51
copper porphyrin[3]	532	1.7
zinc porphyrin[3]	532	1.3
Ni_3HHTP_2[4]	532	4.19
Cu_3HHTP_2[4]	532	1.93
Co_3HHTP_2[4]	532	3.03
Pt-Ni NP/rGO[5]	532	1.92
Pt-Ni NP cluster/rGO[5]	532	1.42
F_{16}PcGa-BP/PMMA[6]	532	2.64
F_{16}PcGaCl/PMMA[6]	532	9.24
TPC[7]	532	1.04
C_{60}[8]	532	12.85
pyrazine-fused trithiasumanene[8]	532	1.78
triselenasumanene[8]	532	2.43
GO[9]	532	2.9
V_2C PMOF (this work)	532	1.27
Ti_3C_2 QD/V_2C PMOF (this work)	532	1.02

Table S3. Linear and NLO parameters of Ti_3C_2 QD, TCPP, V_2C/TCPP, V_2C PMOF, and Ti_3C_2 QD/V_2C PMOF in the ns regime of 532 nm (110 μJ) and in the fs regime of 800 nm (60 nJ). I_0: laser intensity at focus; α_0: linear absorption coefficient; β_{eff}: nonlinear absorption coefficient.

Samples	**Laser**	$\boldsymbol{I_0}$ (μJ)	$\boldsymbol{\beta_{eff}}$ (cm GW^{-1})
Ti_3C_2 QD			3.13 ± 0.55
TCPP	532 nm		124.94 ± 2.27
V_2C/TCPP	12 ns	110	54.29 ± 1.24
V_2C PMOF	10 Hz		483.79 ± 14.79
Ti_3C_2 QD/V_2C PMOF			553.69 ± 19.50
Ti_3C_2 QD			−0.0043 ± 1E-4
TCPP	800 nm		—
V_2C/TCPP	34 fs	0.06	0.0074 ± 4E-4
V_2C PMOF	1 kHz		0.0353 ± 2E-4
Ti_3C_2 QD/V_2C PMOF			0.0495 ± 5E-4

Table S4. NLO parameters of typical MOF, graphene derivatives, and organometallic hybrid materials.

Samples	λ (nm)	I_0 (μJ)	β_{eff} (cm GW^{-1})
TPP[1]	532	8	33
GO[5]	532	50	1.22
Pt NP/rGO[5]	532	50	1.38
Ni NP/rGO[5]	532	50	1.29
Pt-Ni NP/rGO[5]	532	50	1.64
Pt-Ni NP cluster/rGO[5]	532	50	1.98
Mn-TMPP[10]	532	10.3	9
Zn-TMPP[10]	532	10.3	46
Mn-THPP[10]	532	10.3	9
Zn-THPP[10]	532	10.3	18
Co-THPP (crystalline plates)[11]	532	10.3	24
Co-THPP (flower-shaped clusters)[11]	532	10.3	70
Co-THPP (ultrathin films)[11]	532	10.3	95
copper porphyrin[3]	532	0.3 GW cm^{-2}	132
zinc porphyrin[3]	532	0.3 GW cm^{-2}	366
Ni_3HHTP_2[4]	532	155	46
Cu_3HHTP_2[4]	532	155	95
P_1Pt[12]	532	2	39
P_2Pt[12]	532	2	45
ZnP-RGO[13]	532	150	6.58
PF-RGO[13]	532	150	7.07
BP/PMMA[6]	532	400	8.43
F_{16}PcGaCl/PMMA[6]	532	400	74.92
RGO/PMMA[14]	532	300	129.01
PFTP-RGO/PMMA[14]	532	300	215.77
annealed PFTP-RGO/PMMA[14]	532	300	296.79
BP:C_{60} (annealed)[15]	532	40	87.32
BP:C_{60} (annealed)[15]	532	400	241.73
V_2C PMOF (this work)	532	70	483.79
Ti_3C_2 QD/V_2C PMOF (this work)	532	70	553.69

Table S5. NLO parameters of similar heterostructure.

samples	laser	β_{eff} (cm GW^{-1})
PIZA-1-5 film[2]	532 nm, 5 ns, 10 Hz	4.2×10^4
Pt/CND@PCN-222 film[16]	532 nm, 8.5 ns, 10 Hz	6.5×10^4
ZnS/Cu-TCPP[17]	532 nm, 30 ps, 10 Hz	1.73
Cu-MOF/PVP[18]	532 nm, 21 ps, 10 Hz	–22
PPy@Cu-MOF/PVP[18]	532 nm, 21 ps, 10 Hz	77
$[Zn_{2.5}Co_{1.5}(dcpp)_2(DMF)_3(H_2O)_2]_n$[19]	532 nm, 21 ps, 10 Hz	27
$[Zn_{2.5}Co_{1.5}(dcpp)_2(DMF)_3(H_2O)_2]_n$@CeO2[19]	532 nm, 21 ps, 10 Hz	35

2. Theoretical Calculation Methods

All Density Functional Theory (DFT) calculations were performed on the basis of the projector-augmented wave approach in the Cambridge Sequential Total Energy Package. The exchange-correlation function was described by the Perdew-Burke-Ernzerhof generalized gradient approximation using the Tkatchenko-Scheffler method for dispersion correction.[20] The ultrasoft pseudo-potential was used to describe the interactions between valence and core electrons. The planewave kinetic energy cut-off and K-points were set to be 300 eV and 1 × 1 × 1, respectively. Spin polarization was taken into account during the geometry optimization. Geometry optimization for all atoms modules was performed to allow convergence, with thresholds of maximum displacement of 0.002 Å, maximum force of 0.05 eV $Å^{-1}$, maximum stress of 0.1 GPa, and energy of 2.0×10^{-5} eV per atom.

3. Calculation of Nonlinear Absorption Parameters

The total absorption coefficient of the material can be written as:

$$\alpha(I) = -\alpha_0 + \beta I \quad \text{(Equation S1)}$$

where α_0 and β are linear absorption coefficient and nonlinear absorption coefficient, respectively. I is the incident light intensity.

The corresponding light propagation model is expressed as[21]:

$$\frac{dI}{dz} = -(\alpha_0 + \beta I)I \quad \text{(Equation S2)}$$

As for open aperture Z-scan, the normalized transmittance can be given as[21]:

$$T(z) = \sum_{m=0}^{\infty} \frac{\left[\frac{-\beta_{eff} I_0 L_{eff}}{1 + Z^2 / Z_0^2}\right]^m}{(m+1)^{\frac{3}{2}}} \quad \text{(Equation S3)}$$

$$L_{eff} = \frac{(1 - e^{-\alpha_0 L})}{\alpha_0} \quad \text{(Equation S4)}$$

where L_{eff} is the effective interaction length, is the linear absorption coefficient, L is the sample thickness, β_{eff} is the nonlinear absorption coefficient, I_0 is the on-axis peak intensity at the focal plane, and z_0 is the Rayleigh diffraction length. By fitting the experimental data, the nonlinear absorption coefficient β_{eff} can be obtained.

References

[1] Z. Liu, Z. Guo, X. Zhang, J. Zheng, J. Tian, *Carbon* **2013**, 51, 419.
[2] D. Li, Z. Gu, J. Zhang, *Chem. Sci.* **2020**, 11, 1935.
[3] M. B. M. Krishna, V. P. Kumar, N. Venkatramaiah, R. Venkatesan, D. N. Rao, *Appl. Phys. Lett.* **2011**, 98, 081106.
[4] Y. Sun, H. Li, X. Gao, Z. Yu, Z. Huang, C. Zhang, *Adv. Opt. Mater.* **2021**, 9, 2100622.
[5] C. Zheng, L. Lei, J. Huang, W. Chen, W. Li, H. Wang, L. Huang, D. Huang, *J. Mater. Chem. C* **2017**, 5, 11579.
[6] Z. Liu, B. Zhang, N. Dong, J. Wang, Y. Chen, *J. Mater. Chem. C* **2020**, 8, 10197.
[7] M. V. Vijisha, J. Ramesh, C. Arunkumar, K. Chandrasekharan, *J. Mater. Chem. C* **2020**, 8, 12689.
[8] J. Sun, Y. Sun, C. Yan, D. Lin, Z. Xie, S. Zhou, C. Yuan, H.-L. Zhang, X. Shao, *J. Mater. Chem. C* **2018**, 6, 13114.
[9] S. Maharjan, K.-S. Liao, A. J. Wang, Z. Zhu, K. Alam, B. P. McElhenny, J. Bao, S. A. Curran, *Chem. Phys. Lett.* **2019**, 714, 149.
[10] B. W. Xu, R. J. Niu, Q. Liu, J. Y. Yang, W. H. Zhang, D. J. Young, *Dalton Trans* **2020**, 49, 12622.
[11] R. J. Niu, W. F. Zhou, Y. Liu, J. Y. Yang, W. H. Zhang, J. P. Lang, D. J. Young, *Chem Commun.* **2019**, 55, 4873.
[12] Z. Liu, J. Sun, C. Yan, Z. Xie, G. Zhang, X. Shao, D. Zhang, S. Zhou, *J. Mater. Chem. C* **2020**, 8, 12993.
[13] Y. Du, N. Dong, M. Zhang, K. Zhu, R. Na, S. Zhang, N. Sun, G. Wang, J. Wang, *Phys. Chem. Chem. Phys.* **2017**, 19, 2252.
[14] Z. Liu, N. Dong, P. Jiang, K. Wang, J. Wang, Y. Chen, *Chem. Eur. J.* **2018**, 24, 19317.
[15] M. Shi, S. Huang, N. Dong, Z. Liu, F. Gan, J. Wang, Y. Chen, *Chem. Commun.* **2018**, 54, 366.
[16] Y. Xiao, Z. Gu and J. Zhang, *Sci. China Mater.*, 2020, **63**, 1059-1065.
[17] J. L. Humphrey and D. Kuciauskas, *J. Phys. Chem. C*, 2008, **112**, 1700-1704.
[18] J. Huang, F. Lang, Y. Cui, L. Xie, K. Geng, Y. Zhao and H. Hou, *Adv. Opt. Mater.*, 2022, **10**, 2201872.
[19] Y. Sun, W. Xu, F. Lang, H. Wang, F. Pan and H. Hou, *Small*, 2305879.
[20] S. J. Clark, M. D. Segall, C. J. Pickard, P. J. Hasnip, M. I. J. Probert, K. Refson, M. C. Payne, *Z. Krist-Cryst. Mater.* **2005**, 220, 567.
[21] M. Sheik-Bahae, A. A. Said, T. H. Wei, D. J. Hagan, E. W. V. Stryland, *IEEE J. Quantum Elect.* **1990**, 26, 760.